

Pseudo-observables and Deep Neural Network for mixed CP $H \rightarrow \tau\tau$ decays at LHC.

E. Richter-Was^a, T. Yerniyazov^b and Z. Was^c

^a *Institute of Physics, Jagiellonian University, Łojasiewicza 11, 30-348 Kraków, Poland*

^b *Faculty of Physics, Astronomy and Applied Computer Science, Jagiellonian University, Łojasiewicza 11, 30-348 Kraków, Poland*

^c *Institute of Nuclear Physics, IFJ-PAN, Radzikowskiego 152, 31-342 Kraków, Poland*

ABSTRACT

The consecutive steps of cascade decay initiated by $H \rightarrow \tau\tau$ can be useful for the measurement of Higgs couplings and in particular of the Higgs boson parity. The standard analysis method applied so far by ATLAS and CMS Collaborations was to fit a one-dimensional distribution of the angle between reconstructed decay planes of the τ lepton decays, ϕ^* , which is sensitive to transverse spin correlations of the τ decays and, hence, to the CP state mixing angle, ϕ^{CP} .

Machine Learning techniques (ML) offer opportunities to manage such complex multidimensional signatures. The multidimensional signatures, the 4-momenta of the τ decay products can be used directly as input information to the machine learning algorithms to predict the CP-sensitive pseudo-observables and/or provide discrimination between different CP hypotheses. In the previous papers, we have shown that multidimensional signatures, the 4-momenta of the τ decay products can be used as input information to the machine learning algorithms to predict the CP-sensitive pseudo-observables and/or provide discrimination between different CP hypotheses.

In this paper we show how the classification or regression methods can be used to train an ML model to predict the spin weight sensitive to the CP state of the decaying Higgs boson, parameters of the functional form of the spin weight, or the most preferred CP mixing angle of the analysed sample. The one-dimensional distribution of the predicted spin weight or the most preferred CP mixing angle of the experimental data can be examined further, with the statistical methods, to derive the measurement of the CP mixing state of the Higgs signal events in decay $H \rightarrow \tau\tau$.

This paper extends studies presented in our previous publication, with more experimentally realistic scenarios for the features lists and further development of strategies how proposed pseudo-observables can be used in the measurement.

IFJPAN-IV-2024-12

November 2024

T. Y. was supported in part by grant No. 2019/34/E/ST2/00457 of the National Science Center (NCN), Poland and also by the Priority Research Area Digiworld under the program Excellence Initiative Research University at the Jagiellonian University in Cracow.

The majority of the numerical calculations were performed at the PLGrid Infrastructure of the Academic Computer Centre CYFRONET AGH in Kraków, Poland.

1 Introduction

Machine learning techniques are more and more often being applied in high-energy physics data analysis. With Tevatron and LHC experiments, they became an analysis standard. For the recent reviews see e.g. [1, 2, 3].

In this paper, we present how ML techniques can help exploit the substructure of the hadronically decaying τ leptons in the measurement of the Higgs boson CP-state mixing angle ϕ^{CP} in $H \rightarrow \tau\tau$ decay. This problem has a long history [4, 5], and was studied both for electron-positron [6, 7] and for hadron-hadron [8, 9] colliders. Following the proposed by those papers one-dimensional observable, a polar angle ϕ^* between τ leptons decay planes, ATLAS and CMS Collaborations measured the CP mixing angle ϕ^{CP} with Run 2 data collected in pp collisions at LHC. The Standard Model (SM) predicts that the scalar Higgs boson is in the $\phi^{CP} = 0^\circ$ state while the pseudo-scalar would be in the $\phi^{CP} = 90^\circ$ state for the Higgs couplings to τ pairs. The measured value by ATLAS Collaboration [10] is $\phi^{CP} = 9^\circ \pm 16^\circ$, and by CMS Collaboration [11] $\phi^{CP} = -1^\circ \pm 19^\circ$. While data disfavour pure pseudo-scalar coupling with more than 3 standard deviations significance and are compatible with SM expectations of Higgs couplings to τ leptons being scalar-like ($\phi^{CP} = 0$), there is still room for improvement of the precision of the measurement with more data collected during ongoing LHC Run 3 and then even 10 times more data expected with High-Lumi LHC.

The theoretical basis for the measurement is simple, the cross-section dependence on the parity mixing angle has the form of the second-order trigonometric polynomial in the ϕ^{CP} angle. It can be implemented in the Monte Carlo simulations as the per event spin weight wt , which parametrises this sensitivity, see [12] for more details. Even if the problem in its nature is multidimensional: correlations between direction and momenta of the τ lepton decay products, the ML has not been used so far for experimental analysis design. This is in part, because ML adds complexity to the data analysis and requires relatively high statistics of the signal events. Also, the ML solutions need to be evaluated for their suitability in providing estimates of systematic ambiguities.

In [13, 14] we have presented ML-based analysis on the Monte Carlo simulated events for the three channels of the τ lepton-pair decays: $\rho^\pm \nu_\tau \rho^\mp \nu_\tau$, $a_1^\pm \nu_\tau \rho^\mp \nu_\tau$ and $a_1^\pm \nu_\tau a_1^\mp \nu_\tau$. In those papers we limited the scope to the scalar-pseudoscalar classification case. We explored the kinematics of outgoing decay products of the τ leptons and geometry of decay vertices which can be used for reconstructing original τ lepton directions. In the following paper [15], we extended ML analysis to a measurement of the scalar-pseudoscalar mixing angle ϕ^{CP} of the $H \rightarrow \tau\tau$ coupling, limiting it, however, to the ideal situation where the 4-momenta of all outgoing τ decay products were known. In the experimental conditions, this is not the case, because of the two neutrinos from τ decays which cannot be measured directly.

In this paper, we extend further our research to more experimentally realistic representations of $H \rightarrow \tau\tau$ events and focus on using the per-event spin weight wt as a one-dimensional pseudo-observable. We train a machine learning model to predict those weights and relay on for further statistical analysis to infer the ϕ^{CP} mixing angle from predicted distribution. This pseudo-observable can be used as an alternative or complementary to the angle ϕ^* between τ lepton decay planes. As in [15] we still constrain ourselves to the measurement of the coupling in the most promising decay channel $H \rightarrow \tau^+\tau^- \rightarrow \rho^+\nu_\tau\rho^-\nu_\tau \rightarrow \pi^+\pi^0\nu_\tau\pi^-\pi^0\nu_\tau$.

We analyse potential solutions using *deep learning* algorithms [16] and a *Deep Neural Network (DNN)* implemented in the *Tensorflow* environment [17], previously found effective for binary classification [13, 14] between scalar and pseudoscalar Higgs boson hypotheses.

We employ the same DNN architecture used for multiclass classification and regression in [15]. The DNN is tasked with predicting per-event:

- Spin weight as a function of the CP mixing angle ϕ^{CP} .
- Decay configuration dependent coefficients, for the functional form of the spin weight distribution as a function of the mixing angle ϕ^{CP} .
- The most preferred mixing angle, i.e. the value from which the spin weight reaches its maximum.

These goals are complementary or even to a great extent redundant, e.g. with the functional form of the spin weight. We can easily find the mixing angle at which it has a maximum. However, the precision of predicting that value may not be the same for different methods. All three cases are examined as classification and regression problems.

The paper is organised as follows: Section 2 describes the basic phenomenology of the problem. Properties of the matrix elements are discussed and the notation used is introduced. In Section 3 we review feature sets (lists of variables) used as an input to the DNN and present samples prepared for analyses. Section 4 outlines ML methods

and the performance of the DNN. Section 5 delves deeper into the performance across the feature sets with varying levels of realism. Section 6 presents the final discussion on pseudo-observables resulting from the trained DNN and prospects for using them for experimental measurement. Section 7 (Summary) closes the paper.

In Appendix A more technical details on the DNN architecture are given, and input data formulation for classification and regression cases is explained. We also collect figures monitoring the performance of DNN training.

2 Physics description of the problem

The most general Higgs boson Yukawa coupling to a τ lepton pair, expressed with the help of the scalar–pseudoscalar parity mixing angle ϕ^{CP} reads as

$$\mathcal{L}_Y = N \bar{\tau} h (\cos \phi^{CP} + i \sin \phi^{CP} \gamma_5) \tau, \quad (1)$$

where N denotes normalisation, h Higgs field and $\bar{\tau}, \tau$ spinors of the τ^+ and τ^- . As we will see later, this simple analytic form translates itself into useful properties of observable distributions convenient for our goal of determining ϕ^{CP} . Recalling these definitions is therefore justified, aiding in the systematisation of observable quantity (feature) properties and correlations.

The squared matrix element for the scalar/pseudoscalar/mixed parity Higgs, decaying into $\tau^+ \tau^-$ pairs can be expressed as

$$|M|^2 \sim 1 + h_+^i h_-^j R_{i,j}; \quad i, j = \{x, y, z\} \quad (2)$$

where h_{\pm} denote polarimetric vectors of τ decays (solely defined by τ decay matrix elements) and $R_{i,j}$ is the density matrix of the τ lepton pair spin state. Details of the frames used for $R_{i,j}$ and h_{\pm} definition are given in Ref. [18]. The corresponding CP-sensitive spin weight wt has the form:

$$wt = 1 - h_+^z h_-^z + h_+^{\perp} R(2\phi^{CP}) h_-^{\perp}. \quad (3)$$

The formula is valid for h_{\pm} defined in τ^{\pm} rest-frames, h^z stands for longitudinal and h^{\perp} for transverse components of h . The $R(2\phi^{CP})$ denotes the $2\phi^{CP}$ angle rotation matrix around the z direction: $R_{xx} = R_{yy} = \cos 2\phi^{CP}$, $R_{xy} = -R_{yx} = \sin 2\phi^{CP}$. The τ^{\pm} decay polarimetric vectors h_+^i, h_-^j , in the case of $\tau^{\pm} \rightarrow \pi^{\pm} \pi^0 \nu$ decay, read

$$h_{\pm}^i = \mathcal{N} \left(2(q \cdot p_{\nu}) q^i - q^2 p_{\nu}^i \right), \quad (4)$$

where τ decay products π^{\pm}, π^0 and ν_{τ} 4-momenta are denoted respectively as $p_{\pi^{\pm}}, p_{\pi^0}, p_{\nu}$ and $q = p_{\pi^{\pm}} - p_{\pi^0}$. Obviously, complete CP sensitivity can be extracted only if p_{ν} is known.

Note that the spin weight wt is a simple first-order trigonometric polynomial in a $2\phi^{CP}$ angle. This observation is valid for all τ decay channels. For the clarity of the discussion on the DNN results, we introduce $\alpha^{CP} = 2\phi^{CP}$, which spans over $(0, 2\pi)$ range. $\alpha^{CP} = 0, 2\pi$ corresponds to the scalar state, while $\alpha^{CP} = \pi$ corresponds to the pseudoscalar one. The spin weight can be expressed as

$$wt = C_0 + C_1 \cdot \cos(\alpha^{CP}) + C_2 \cdot \sin(\alpha^{CP}), \quad (5)$$

where coefficients

$$\begin{aligned} C_0 &= 1 - h_+^z h_-^z, \\ C_1 &= -h_+^x h_-^x + h_+^y h_-^y, \\ C_2 &= -h_+^x h_-^y - h_+^y h_-^x, \end{aligned} \quad (6)$$

depend on the τ decays only. Distribution of the C_0, C_1, C_2 coefficients, for the sample of $H \rightarrow \tau\tau$ events used for our numerical results is shown in Figure 1. The C_0 spans $(0, 2)$ range, while C_1 and C_2 of $(-1, 1)$ range have a similar shape, quite different than the one of C_0 .

The amplitude of the spin weight wt as a function of α^{CP} depends on the multiplication of the length of the transverse components of the polarimetric vectors. The longitudinal component $h_+^z h_-^z$ defines shift with respect to

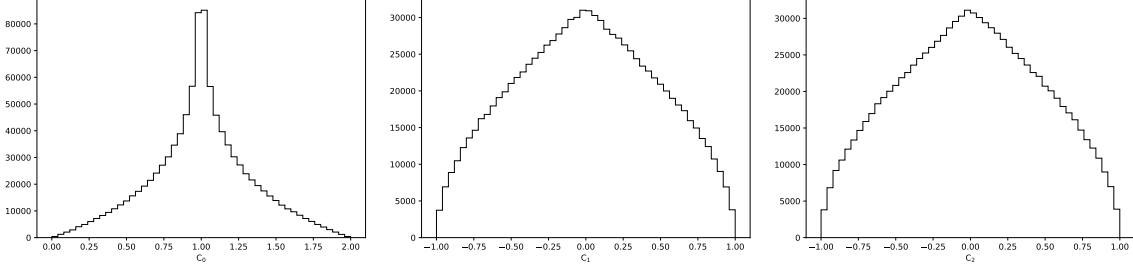


Figure 1: Distributions of the C_0, C_1, C_2 coefficients of formula (5), for the $H \rightarrow \tau\tau$ events sample.

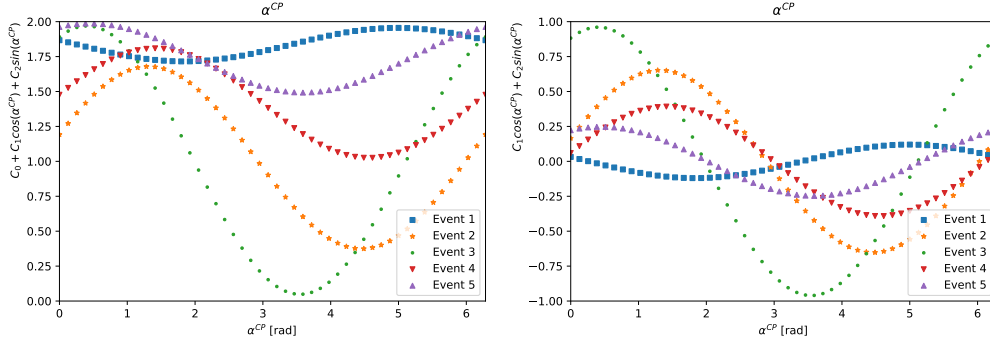


Figure 2: The spin weight wt (left plot) and only its α^{CP} dependent component (right plot) for a few $H \rightarrow \tau\tau$ events. Note the vertical scale difference between the plots due the inclusion of the C_0 term in the left plot and its absence in the right.

zero of the wt mean value and is constant over a full $(0, 2\pi)$ range of α^{CP} . The wt distribution maximum is reached for $\alpha^{CP} = \angle(h_+^T, h_-^T)$, the opening angle of the transverse components of the polarimetric vectors.

The spin weight wt of the formula (5) can be used to introduce transverse spin effects into the event sample when for the generation transverse spin effects were not taken into account at all. The above statement holds true regardless of whether longitudinal spin effects were included and which τ decay channels complete cascade of $H \rightarrow \tau\tau$ decay. The shape of weight dependence on the Higgs coupling to the τ parity mixing angle is preserved.

In Fig. 2 we show the distribution of the spin weight wt for five example $H \rightarrow \tau\tau$ events. For each event, a single value of α^{CP} is the most preferred (corresponding to the largest weight), determined by its polarimetric vectors.

3 Monte Carlo samples and feature sets

For compatibility with our previous publications [13, 14, 15], we use the same samples of generated events, namely Monte Carlo events of the Standard Model, 125 GeV Higgs boson, produced in pp collision at 13 TeV centre-of-mass energy, generated with `Pythia 8.2` [20], with τ leptons decays simulated with the `Tauolapp` library [21]. Samples are generated without spin correlations included, each τ lepton is decayed independently.

The spin effects are introduced with the spin weight wt calculated with the `TauSpinner` [22, 12, 23] package, for several different hypotheses of the CP mixing angle α_i^{CP} and stored together with information on τ leptons decay products. The spin weight (3), is calculated using $R_{i,j}$ density matrix and polarimetric vectors h_\pm , as explained in the previous Section. In the process of the analysis, for a given event it is possible to restore the information of the per-event coefficients C_0, C_1, C_2 , using its value of the spin weight wt at three α^{CP} hypotheses and solving the linear equation (5) or fitting the (5) formula.

In this paper we present results for the case when both τ decays $\tau^\pm \rightarrow \rho^\pm \nu_\tau$ and about 10^6 simulated Higgs events are used. To partly emulate detector conditions, a minimal set of cuts is used. We require that the transverse momenta

Table 1: The feature sets used as inputs to ML algorithms, categorised by `Variant-X.Y` family. The third column number indicates the number of features for the $\rho^\pm - \rho^\mp$. All 4-vectors components are calculated in the rest frame of the hadronic decay products.

Notation	Features	Counts	Comments
Variant-All	4-vectors (π^\pm, π^0, ν)	24	
Variant-1.1	4-vectors $(\pi^\pm, \pi^0, \rho^\pm), m_i^2, m_k^2, y_i, y_k, \phi_{i,k}^*$	29	
Variant-4.1	4-vectors (π^\pm, π^0) , 4-vectors τ	24	Approx. p_τ

of the visible decay products combined, for each τ , are larger than 20 GeV. It is also required that the transverse momentum of each π^\pm is larger than 1 GeV.

The emphasis of the paper is to explore the feasibility to learn spin weight wt or its components C_0, C_1, C_2 with ML techniques. For the ML training as feature sets (quantities) we consider few scenarios introduced in paper [14]. We discuss the case of an idealistic benchmark scenario with the `Variant-All` feature set, where the four-momenta of *all* decay products of τ leptons are defined in the rest frame of intermediate resonance pairs ($\rho - \rho$ system). Scenarios which are more realistic in experimental conditions rely on the information that could be reconstructed from experimental data. The first one, `Variant-1.1`, is based on the 4-vectors and their products for visible decay products only. The second one, `Variant-4.1`, includes some approximate information on the original τ lepton direction.

Table 1 details the feature sets of the considered models. For more details on the specific frames and approximations used for representing neutrinos or τ lepton 4-momenta, please refer to [14]. We do not introduce any additional energy or momentum smearing, leaving the evaluation of its impact to experimental analysis.

4 Training and evaluation: *Variant-All*

We start by discussing results for an idealistic case, i.e. the *Variant-All* feature set. This reminds us to a great extent what was previously reported in the scope of [15].

4.1 Learning spin weights wt

The DNN classifier is trained on a per-event feature set to predict an N_{class} -dimensional per-event vector of spin weights normalised to probability. Each component of the $wt^{norm}(\alpha^{CP})$ vector is a weight associated with a discrete value of the mixing angle α_i^{CP} . N_{class} represents the number of discrete points into which the range $(0, 2\pi)$ is divided. To guarantee that α^{CP} values of 0, π and 2π (corresponding to scalar, pseudoscalar, and again scalar states, respectively) are always included as distinct classes, the total number of classes, N_{class} , is maintained as an odd number. As baseline, the DNN is trained with N_{class} set to 51.

Similarly, in the regression case, the DNN is trained on per-event feature sets with the corresponding spin weight vector, wt_i , for discrete α^{CP} values as the target variable. The DNN learns both shape and normalisation of the wt vector during the training.

We quantify the DNN performance using physics-relevant criteria. The primary metric is the ability of the DNN to reproduce the per-event spin weight, wt^{norm} . Figure 3 illustrates the true and predicted wt^{norm} distributions for two example events as a function of the class index i (representing the discretised mixing parameter α_i^{CP}). The blue line indicates true spin weights, while the orange line represents weights predicted by the DNN classifier. Generally, the DNN accurately predicts the spin weight for some events, but struggles for others. Encouragingly, the predicted weights exhibit the expected smooth, linear combination of $\cos(\alpha^{CP})$ and $\sin(\alpha^{CP})$. This is notable given that the loss function does not explicitly correlate nearby classes, indicating the capacity of the DNN to learn this pattern during training.

The second criterion is the difference between the most probable predicted class and the most probable true class, denoted as Δ_{class} . When calculating the difference between class indices, the periodicity of the functional form (Equation (5)) is considered. Class indices represent discrete values of α^{CP} within the range $(0, 2\pi)$. The distance

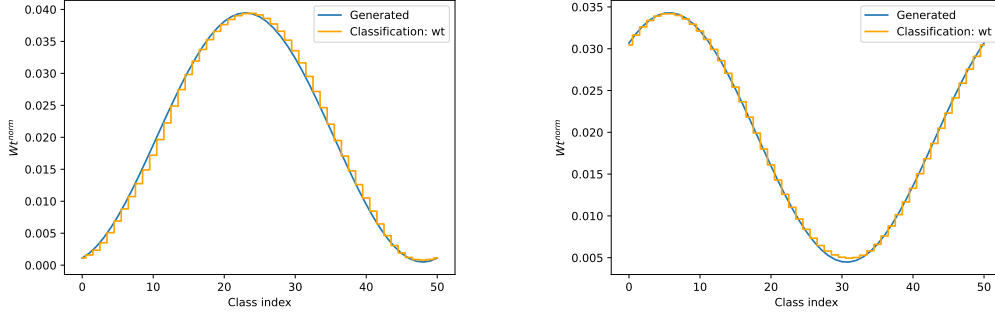


Figure 3: Normalised spin weight, wt^{norm} , predicted (orange line) and true (blue line), as a function of the class index for two example events. The DNN was trained using the classification method with $N_{class} = 51$ and *Variant-All*.

between the first and the last class is zero. We compute the distance corresponding to the smaller angle difference and assign a sign based on the clockwise orientation relative to the class index where the true wt reaches its maximum.

From a physics perspective, learning the shape of the wt distribution as a function of α^{CP} is equivalent to learning the components of the polarimetric vectors. Note Ref. [24] for the possible extension of the methods for other τ decay channels. For learning the polarimetric vectors the much larger $Z \rightarrow \tau\tau$ sample can be used too.

However, since only the shape, not the normalisation, is available, the C_i coefficients cannot be fully recovered from wt^{norm} . This is not the primary goal, though. The physics interest lies in determining the preferred α^{CP} value for events in the analysed sample, i.e. the value where the summed wt distribution reaches its maximum. This aligns with the objective of potential measurement, namely, determining the CP mixing of the analysed sample, which will be discussed further in Section 6.

Figure 5, top-left panel, displays the distribution of Δ_{class} for $N_{class} = 51$ for the DNN trained with the classification method and *Variant-All/4.1/1.1*. The distribution is Gaussian-like and centered around zero with standard deviation $\sigma_{\Delta_{class}} = 0.179$ [rad] for *Variant-All*. The top-right panel of Figure 5 shows the distribution of Δ_{class} for $N_{class} = 51$ using the regression method. In this case, $\sigma_{\Delta_{class}} = 0.170$ [rad] for *Variant-All*. Our findings indicate that the accuracy of learning the spin weight wt using classification and regression methods is comparable.

4.2 Learning C_0, C_1, C_2 coefficients

The second approach involves learning the C_0, C_1, C_2 coefficients of formula (5) for the spin weight wt . Once learned, these coefficients can be used to predict wt and wt^{norm} for a given α^{CP} hypothesis. The coefficients C_0, C_1 , and C_2 represent physical observables, being the products of longitudinal and transverse components of polarimetric vectors, as detailed in formulas (6).

The classification technique using the DNN is configured to learn each C_i independently. The allowed ranges for these coefficients are well-established: C_0 spans (0.0, 2.0) and C_1, C_2 span $(-1.0, 1.0)$, as illustrated in Figure 1. The allowed ranges for these coefficients are divided into N_{class} bins, and each event is assigned an N_{class} -dimensional one-hot encoded vector representing the corresponding C_i value and serving as a label. In this setup, a single class corresponds to a specific C_i coefficient value. During training, the DNN learns to associate per-event features with these class labels. The output is a probability distribution over the N_{class} values, which is converted to a one-hot encoded representation, selecting the most probable class as the predicted C_i value.

The regression method learns all three C_0, C_1 , and C_2 coefficients simultaneously. The learning accuracy is comparable to that of the classification method.

We utilise the true and predicted C_0, C_1 , and C_2 coefficients to compute the wt distribution according to formula (5). This distribution is then discretised into N_{class} points (potentially different from the N_{class} used for learning coefficients), and the α_{max}^{CP} is determined based on the class with the maximum weight. The difference between the true and predicted α_{max}^{CP} is shown in the middle row of Figure 5 for $N_{class} = 51$, comparing classification (left) and regression (right) methods. The Gaussian-like shape of these distributions, centered around zero, clearly demonstrates successful method performance for *Variant-All*. The mean and standard deviation of these distributions are close to

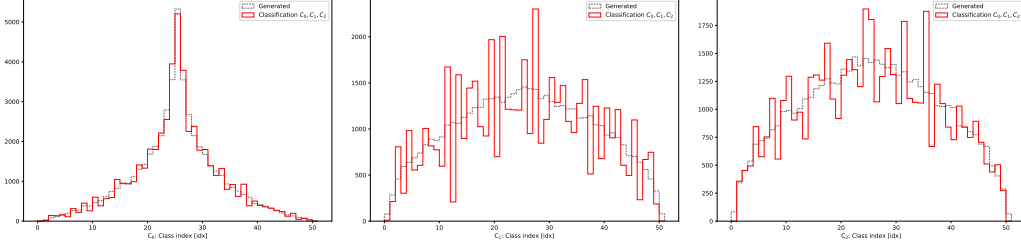


Figure 4: Distributions of true and predicted C_0, C_1 , and C_2 coefficients from formula (6). The DNN was trained using the classification method with $N_{class} = 51$ and *Variant-All*.

Table 2: Mean and standard deviation of the per-event difference ($\Delta\alpha_{max}^{CP}$) between true and predicted α_{max}^{CP} values, obtained from DNN classification and regression methods for *Variant-All*, *Variant-4.1*, and *Variant-1.1*.

Method	Classification Variants: All / 4.1 / 1.1	Regression Variants: All / 4.1 / 1.1
Using wt	std = 0.179 / 0.714 / 1.393 [rad]	std = 0.170 / 0.704 / 1.391 [rad]
Using C_0, C_1, C_2	std = 0.248 / 0.748 / 1.399 [rad]	std = 0.164 / 0.681 / 1.394 [rad]
Direct	std = 0.169 / 0.745 / 1.414 [rad]	std = 0.543 / 0.883 / 1.396 [rad]

those obtained with the `Classification:wt` approach.

4.3 Learning the α_{max}^{CP}

The third approach is to learn the per-event most preferred mixing angle, α_{max}^{CP} , directly. For classification, the allowed range $(0, 2\pi)$ is again divided into N_{class} bins, where each bin represents a discrete α^{CP} value. A one-hot encoded N_{class} -dimensional vector, indicating the true α^{CP} value for each event, serves as the training label. The DNN outputs an N_{class} -dimensional probability vector, from which the class with the highest probability is selected as the predicted α_{max}^{CP} . Notably, this approach bypasses the prediction of the spin weight or C_i coefficients. The regression method implementation allows us to learn the per-event most preferred mixing angle, α_{max}^{CP} , as a continuous value without having to deal with discretised predictions.

The difference between the true and predicted α_{max}^{CP} , denoted as $\Delta\alpha_{max}^{CP}$, is shown in the bottom plot of Figure 5 for both classification (left) and regression (right) methods. The distribution for classification is Gaussian-like with a standard deviation of 0.169 [rad] for *Variant-All*. Regression demonstrates worse performance.

5 Training and evaluation: *Variant-XX*

For *Variant-All*, the information accessible for DNN training is identical to that used for calculating weights wt . Rather than employing mathematical formulas, the DNN learns to recognise patterns in the expected wt values. In contrast, for other *Variant-XX* feature sets, while the true value for training is computed using complete event decay information, the input of the DNN is restricted. Specific details can be found in Table 1.

Table 2 compares performance on the most critical metric: the difference between the true and predicted per-event spin weight wt or the true and predicted most preferred α_{max}^{CP} where the spin weight of the event peaks. While the information provided to the DNN is reduced gradually from *Variant-4.1* to *Variant-1.1*, performance deteriorates.

Variant-1.1 offers sufficient information to calculate the α^{CP} -sensitive observable ϕ^* and also includes this observable explicitly, but falls short in training the DNN to accurately learn variables directly tied to polarimetric vectors: the spin weight wt and coefficients C_0, C_1 , and C_2 . As shown in Equation (4), polarimetric vectors rely on neutrino directions which are experimentally undetectable. Introducing approximations for neutrino information within feature sets, as in *Variant-4.1*, enhances prediction accuracy.

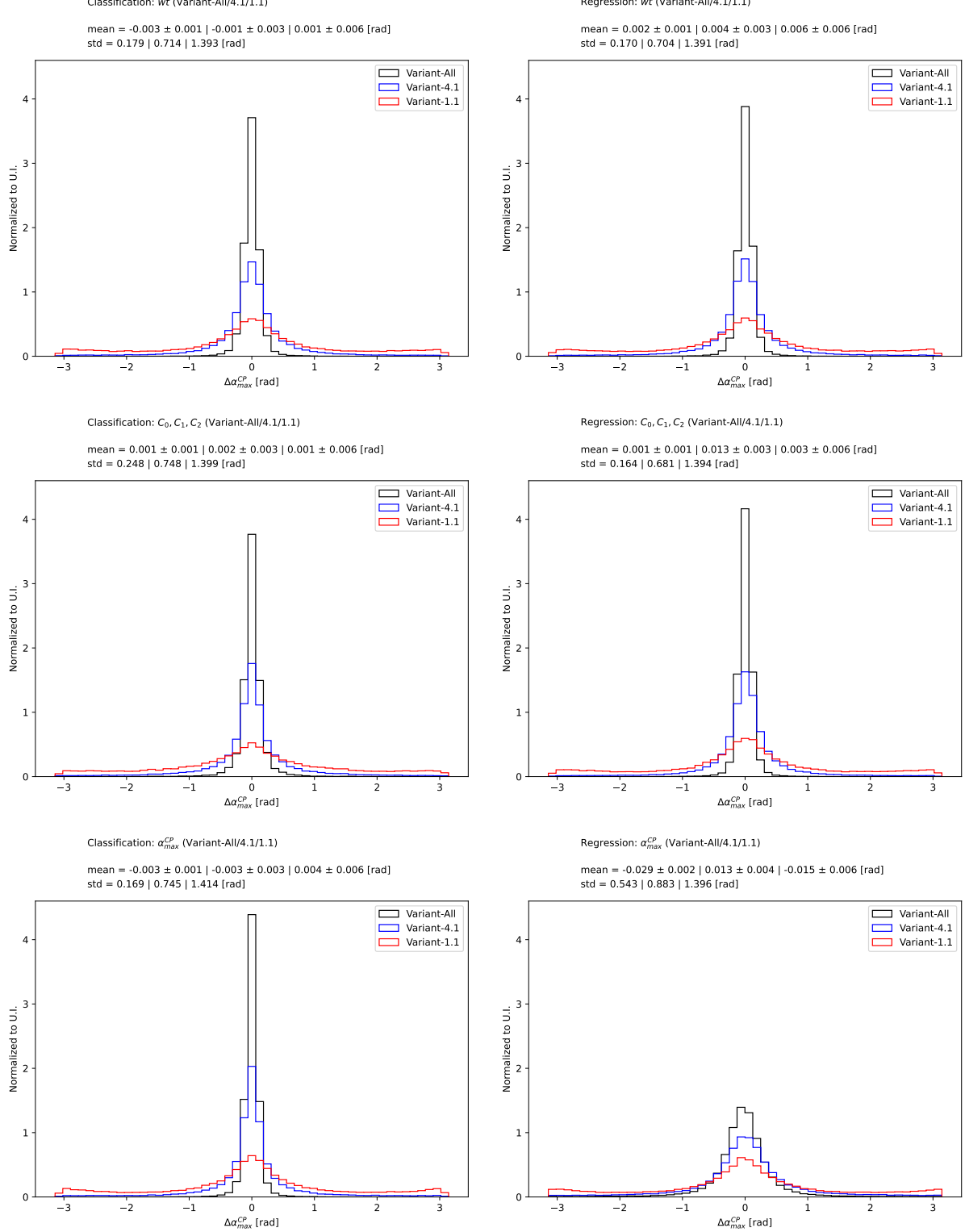


Figure 5: Distribution of the per-event difference between true and predicted α_{max}^{CP} , obtained using: (top row) spin weight learned via classification (left) and regression (right); middle row: spin weight calculated using formula 5 and C_0, C_1 , and C_2 coefficients learned via classification (left) and regression (right); bottom row: direct comparison of true and predicted α_{max}^{CP} using classification (left) and regression (right). The DNN was trained with $N_{class} = 51$ and *Variant-All*, *Variant-4.1*, *Variant-1.1*.

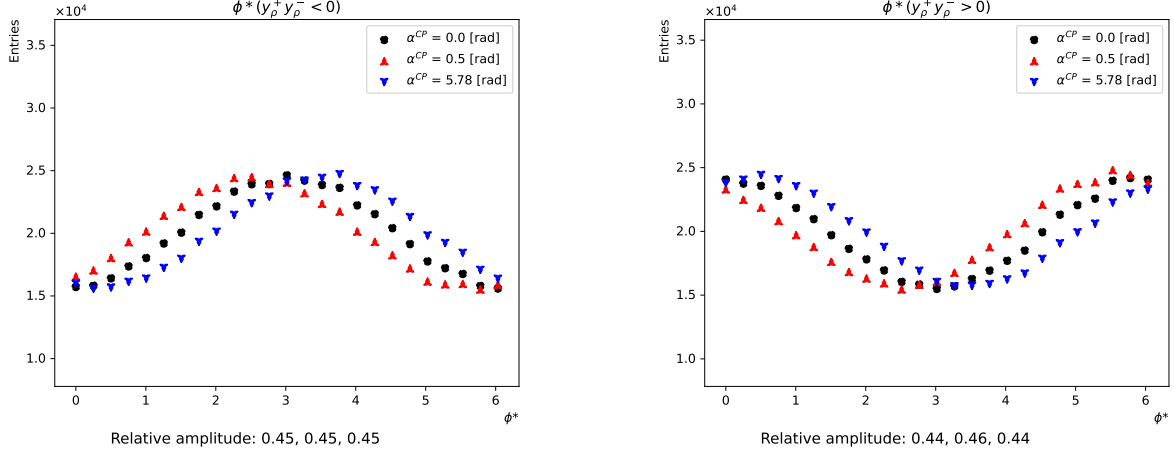


Figure 6: The ϕ^* distribution for three α^{CP} hypotheses, $\alpha^{CP} = -29^\circ, 0^\circ, 29^\circ$.

6 Results with pseudo-experiments

The experimental measurements published by ATLAS [10] and CMS [11] Collaborations rely on fitting the one-dimensional distribution of ϕ^* , defined as the angle between the τ decay planes. This angle is sensitive to the transverse spin correlations between decaying τ leptons and consequently to the CP state of the Higgs boson in $H \rightarrow \tau\tau$ decays.

The calculation of ϕ^* depends on the τ lepton decay modes and was developed for hadron colliders in papers [8, 9]. It is based on the four-momenta of the visible τ decay products and, in the case of the $\tau \rightarrow \pi^\pm \nu$ decay, on the impact parameter of the decay vertex. The ϕ^* distribution for a sample of events with a given α^{CP} mixing state exhibits a characteristic first-order trigonometric polynomial shape, with the maximum value linked to an α^{CP} hypothesis. Following the convention used in publications, the maximum is located at $\phi^* = 90^\circ$ for the scalar case and at $\phi^* = 0^\circ, 180^\circ$ for the pseudoscalar case. The position of the maximum shifts according to the linear relation $\Delta\phi^* = 2\Delta\alpha^{CP}$.

Here, we employ the definition developed much earlier [5, 13], specifically tailored for $\tau \rightarrow \rho\nu$ decays. Figure 6 shows the ϕ^* distribution for events used in this analysis for three different hypotheses: $\alpha^{CP} = -29^\circ, 0^\circ, 29^\circ$, with the middle one corresponding to the scalar Higgs case.

6.1 Distribution of the spin weight wt

In this paper, we propose an alternative or complementary observable, the spin weight wt distribution, which represents the probability of an event occurring for a given α^{CP} hypothesis. The position of the maximum of the wt distribution for a series of events indicates the α^{CP} mixing value for that series. As discussed in previous sections, we can train DNN algorithms on Monte Carlo events to predict the per-event spin weight wt for different α^{CP} hypotheses. Subsequently, we can apply the trained algorithm to experimental data to predict the spin weight wt and obtain its distribution within the analysed sample. Statistical analysis of this distribution (one-dimensional fit) can yield a measurement of the most probable α^{CP} mixing value and, consequently, the CP state of the $H \rightarrow \tau\tau$ coupling.

For the numerical “proof of concept” presented in this paper, we used a Monte Carlo unweighting technique to isolate event series corresponding to specific α^{CP} hypotheses. For each series, the trained DNN predicted the per-event spin weight wt as a function of different α^{CP} hypotheses, using either classification or regression methods. The distribution of the summed spin weights, Σwt , served as a one-dimensional observable for measuring the most probable α^{CP} mixing state.

Figures 7 to 9 show, for the same unweighted event series corresponding to α^{CP} hypotheses with indices $idx = 0, 4, 46$ (from the range $(0, 50)$), the sum of predicted per-event spin weights Σwt as a function of α^{CP} for different feature sets. While the *Variant-4.1* feature set demonstrates relatively accurate prediction of wt dependence on the α^{CP} hypothesis, the *Variant-1.1* exhibits a washed-out sensitivity to discriminate between hypotheses. Predicted per-event

Table 3: Amplitude of the Σwt distribution ($idx = 4$) obtained from DNN classification and regression methods for *Variant-All*, *Variant-4.1*, and *Variant-1.1*.

Method	Classification Variants: All / 4.1 / 1.1	Regression Variants: All / 4.1 / 1.1
Using wt	44% / 35% / 12%	44% / 33% / 11%
Using C_0, C_1, C_2	41% / 33% / 16%	44% / 35% / 13%

weights become flatter for most events shown in the left column of Figure 8, resulting in a preferred α^{CP} hypothesis (index idx with maximum Σwt) shifted by one. This aligns with our earlier observations on training performance for different feature sets in Section 5.

The plots in Figures 7 to 9 also reveal the relative amplitude of Σwt , which diminishes as we move from *Variant-All* to *Variant-1.1* due to reduced information in the input feature set.

Table 3 summarises the sensitivity of the Σwt observable, quantified as the amplitude in the distribution as a function of the α^{CP} hypothesis. Amplitude is defined as $(max - min)/((max + min)/2)$ of the Σwt value for a series of events with a given α^{CP} hypothesis.

7 Summary

We have presented a proof-of-concept study applying DNN methods to measure the Higgs boson $H \rightarrow \tau\tau$ CP-mixing angle-dependent coupling. This work extends the previous research on classifying scalar and pseudoscalar Higgs CP states (Refs. [13, 14]) and builds upon our earlier work on developing classification and regression algorithms, in which some numerical results were collected (Ref. [15]).

We have proposed using the per-event spin weight learned with DNN algorithms as a sensitive observable for measuring the Higgs boson $H \rightarrow \tau\tau$ CP-mixing angle coupling. This approach offers an alternative or complement to the commonly used ϕ^* angle, defined as the polar angle between reconstructed τ lepton decay planes. The ϕ^* angle has been used as a one-dimensional variable in recent ATLAS [10] and CMS [11] measurements, where a template fit was applied to extract the ϕ^{CP} value. However, it requires dedicated, per-decay mode combination algorithms to reconstruct ϕ^* angle from the kinematics of detectable τ lepton decay products. The existing algorithms might not be optimal, and their development becomes even more challenging for cascade decays involving intermediate resonances that decay into multi-body final states. Using the sum of predicted wt distribution in series of events, as a function of α_{CP} hypothesis seems like a very interesting and promising option.

We have extended the work of [15] by investigating more realistic feature sets for the DNN training and focusing on predicting the shape of the spin weight distribution, not just the most probable α^{CP} mixing angle. For this "proof-of-concept" study, we have considered only the dominant and most sensitive decay mode, $\tau \rightarrow \rho^\pm \nu$. We compare an idealised feature set, assuming complete knowledge of τ decay product four-momenta including neutrinos, to more realistic scenarios where only visible decay products are reconstructed or approximations are made for neutrinos or initial τ lepton momenta.

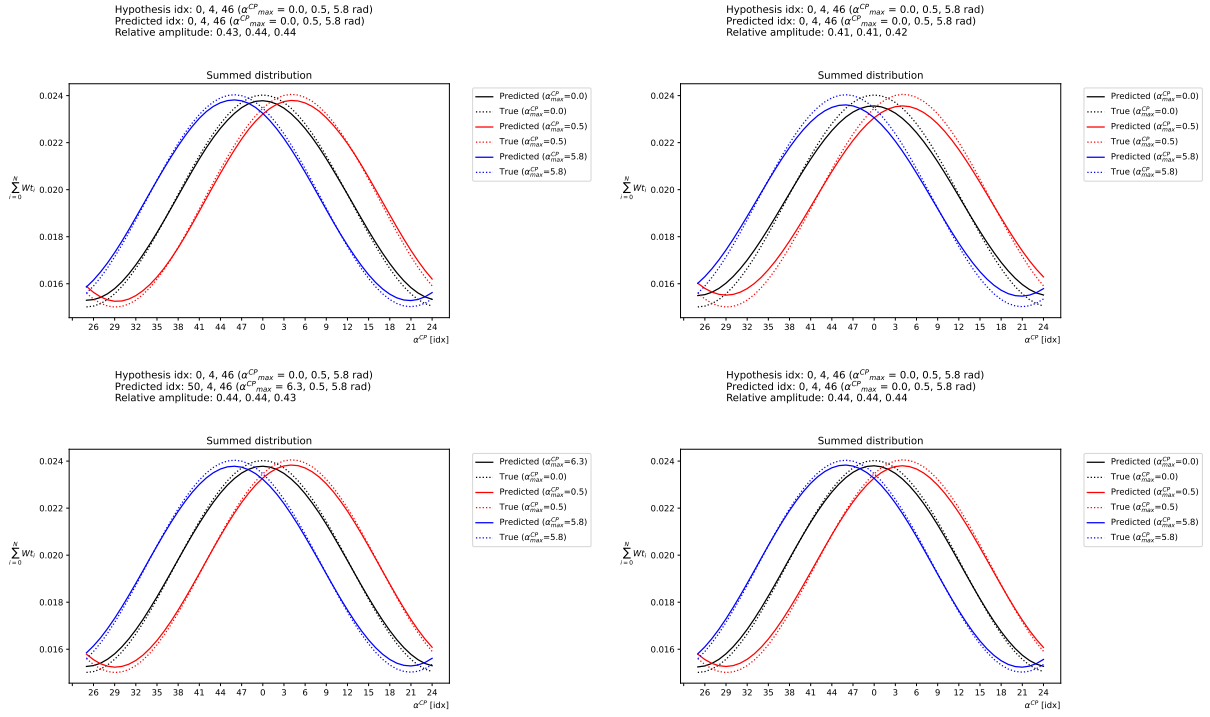


Figure 7: Summed true and predicted per-event spin weights, $\sum wt$, as a function of α^{CP} for the same series of events unweighted to α^{CP} hypotheses with $\alpha^{CP} = -29^\circ, 0^\circ, 29^\circ$. Results are shown for Classification:weights (top-left), Classification: C_0, C_1, C_2 (top-right), Regression:weights (bottom-left), and Regression: C_0, C_1, C_2 (bottom-right) methods using the *Variant-All* feature set for DNN training.

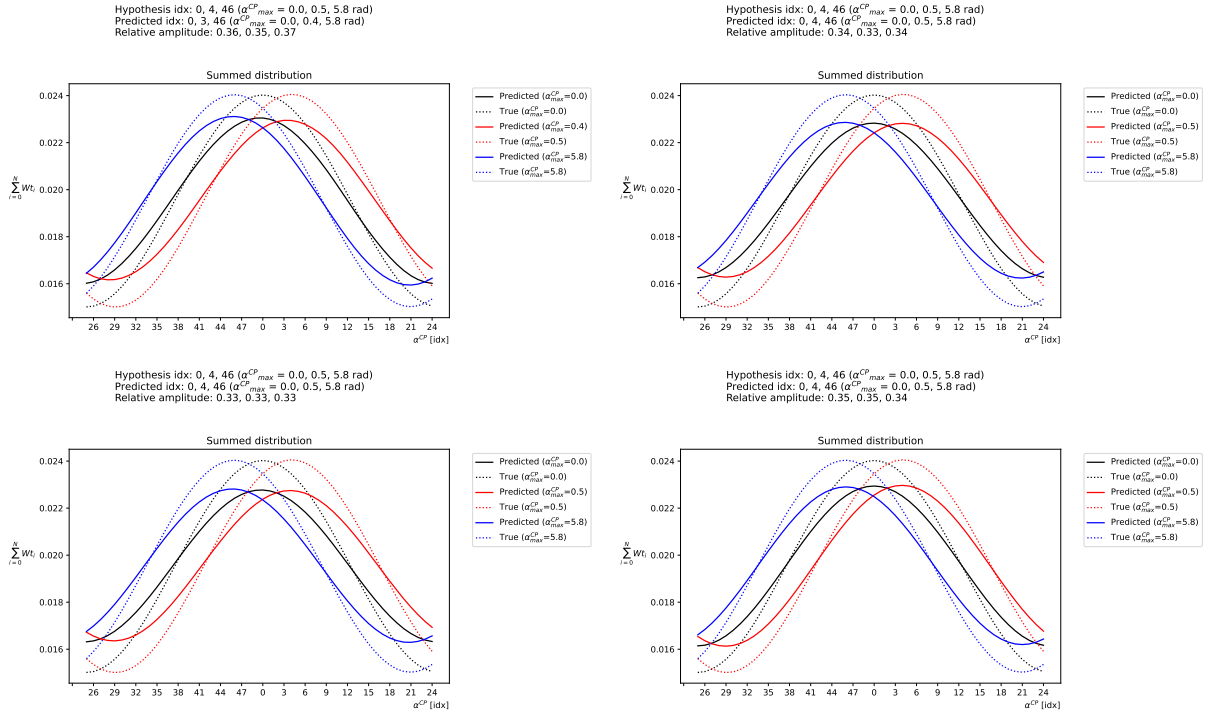


Figure 8: Summed true and predicted per-event spin weights, $\sum wt$, as a function of α^{CP} for the same series of events unweighted to α^{CP} hypotheses with $\alpha^{CP} = -29^\circ, 0^\circ, 29^\circ$. Results are shown for Classification:weights (top-left), Classification: C_0, C_1, C_2 (top-right), Regression:weights (bottom-left), and Regression: C_0, C_1, C_2 (bottom-right) methods using the *Variant-4.1* feature set for DNN training.

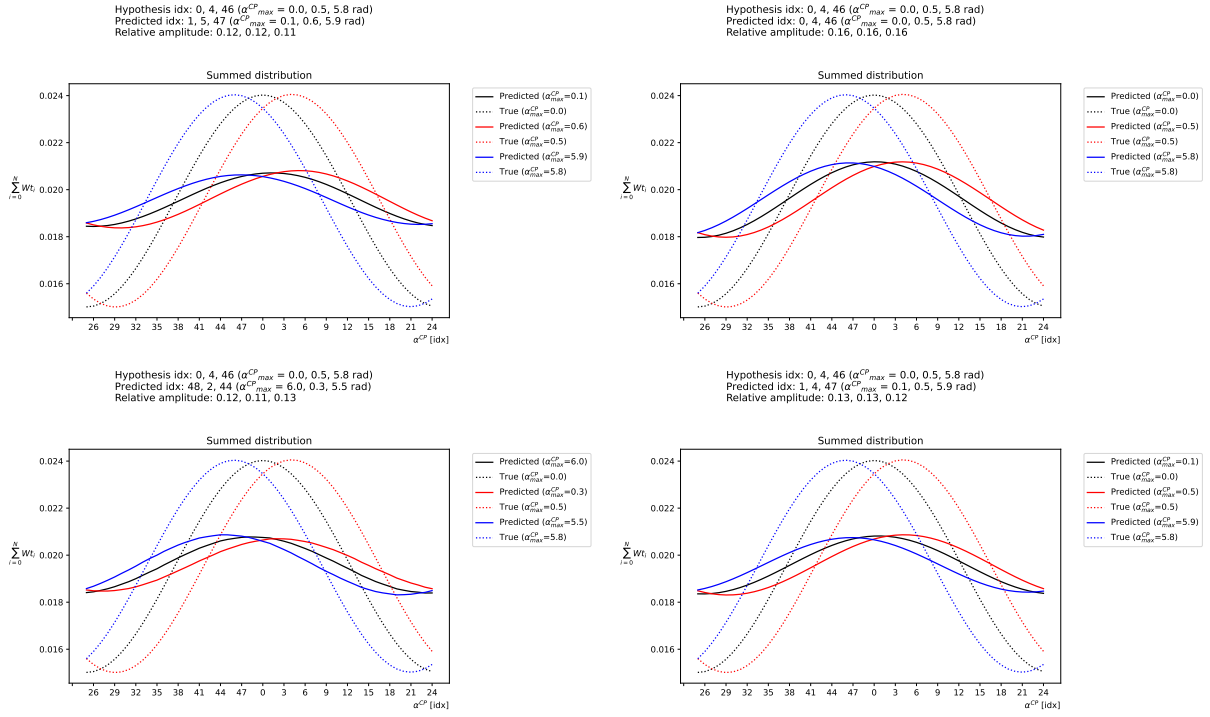


Figure 9: Summed true and predicted per-event spin weights, $\sum wt$, as a function of α^{CP} for the same series of events unweighted to α^{CP} hypotheses with $\alpha^{CP} = -29^\circ, 0^\circ, 29^\circ$. Results are shown for Classification: weights (top-left), Classification: C_0, C_1, C_2 (top-right), Regression: weights (bottom-left), and Regression: C_0, C_1, C_2 (bottom-right) methods using the *Variant-1.1* feature set for DNN training.

A Neural Network

A.1 Architecture

The structure of the simulated data and the DNN architecture follows what was published in our previous papers [13, 14, 15]. We use open-source libraries, TensorFlow [17] and Keras [25], to implement the models, and SciPy [26] to compute the set of C_i coefficients while preparing data sets.

We consider the $H \rightarrow \tau\tau$ channel and both $\tau^\pm \rightarrow \rho^\pm \nu$ decays. Each data point represents an event of Higgs boson production and τ lepton pair decay products. The structure of the event is represented as follows:

$$x_i = (f_{i,1}, \dots, f_{i,D}), w_{a_i}, w_{b_i}, \dots, w_{m_i} \quad (7)$$

The $f_{i,1}, \dots, f_{i,D}$ represent numerical features, and $w_{a_i}, w_{b_i}, w_{m_i}$ are weights proportional to the likelihoods that an event comes from a class A, B, \dots, M , each representing a different α^{CP} mixing angle. The $\alpha^{CP} = 0, 2\pi$ corresponds to the scalar CP state, and $\alpha^{CP} = \pi$ corresponds to the pseudoscalar CP state. The weights calculated from the quantum field theory matrix elements are available and stored in the simulated data files. This is a convenient situation, which does not occur in many other cases of ML classification. The A, B, \dots, M distributions highly overlap in the $(f_{i,1}, \dots, f_{i,D})$ space.

Two techniques have been used to measure the Higgs boson CP state: multiclass classification and regression:

- For multiclass classification (Figure 10), the aim is to simultaneously learn weights (probabilities) for several $\mathcal{H}_{\alpha^{CP}}$ hypotheses, learn coefficients of the weight functional form, or directly learn the mixing angle at which the spin weight has its maximum, α_{max}^{CP} . A single class can be either a single discretised α^{CP} or C_i coefficient value. The system learns the probabilities for classes to be associated with the event.
- For the regression case (Figure 11), the aim is similar to the multiclass classification case, but now the problem is defined as a continuous case. The system learns a value to be associated with the event. The value can be a vector of spin weights for a set of $\mathcal{H}_{\alpha^{CP}}$ hypotheses, a set of C_i coefficients or α_{max}^{CP} .

The network architecture consists of 6 hidden layers, each with 100 nodes, undergoing batch normalisation [27], followed by the ReLU activation function. Model weights are initialised randomly. We use Adam [28] as an optimiser.

The last layer is specific to the implementation case, differing in dimension of the output vector, activation function, and loss function. The details are described below.

Classification: The loss function used in stochastic gradient descent is the cross-entropy of valid values and neural network predictions. The loss function for a sample of N_{evt} events and classification for N_{class} classes reads as follows:

$$Loss = - \sum_{k=1}^{N_{evt}} \sum_{i=1}^{N_{class}} y_{i,k} \ln(p_{i,k}), \quad (8)$$

where k stands for consecutive events and i for the class index. The $p_{i,k}$ represents the neural network predicted probability for event k being of class i , while $y_{i,k}$ represents the true probability used in supervised training.

Regression: In the case of predicting wt , the last layer is N -dimensional output (the granularity with which we want to discretise it). For predicting C_0, C_1, C_2 , the last layer is $N = 3$ dimensional output, i.e. values of C_0, C_1, C_2 . Activation of this layer is a linear function. The loss function is defined as the Mean Squared Error (MSE) between true and predicted parameters:

$$Loss = \sum_{k=1}^{N_{evt}} \sum_{i=1}^{i=N} (y_{i,k} - p_{i,k})^2, \quad (9)$$

where k stands for the event index and i for the index of the function form parameter. The $p_{i,k}$ represents the predicted value of the C_i - th parameter for event k while $y_{i,k}$ represents the true value.

For predicting α_{max}^{CP} , the last layer is $N = 1$ dimensional output, i.e. values of α_{max}^{CP} , with the loss function:

$$Loss = \sum_{k=1}^{N_{evt}} (1 - \cos(y_k - p_k)), \quad (10)$$

where p_k and y_k denote the predicted and true value of α_{max}^{CP} , respectively.

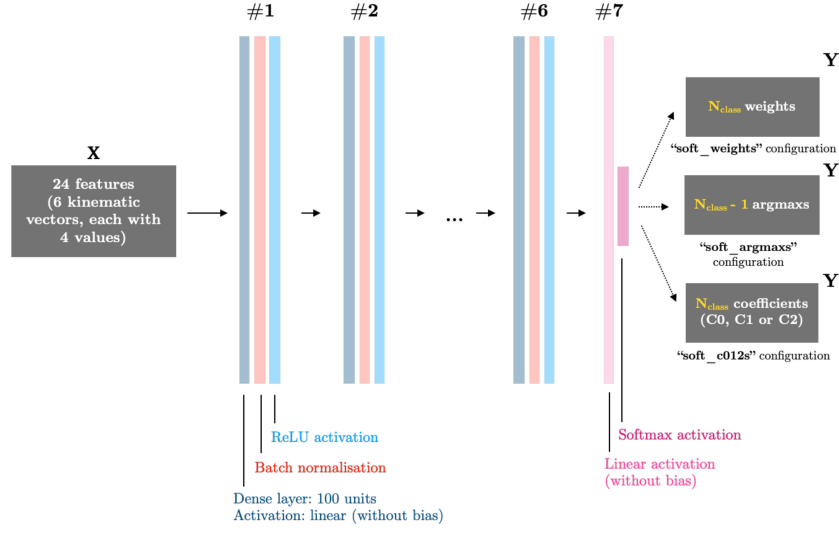


Figure 10: Architecture of classification models

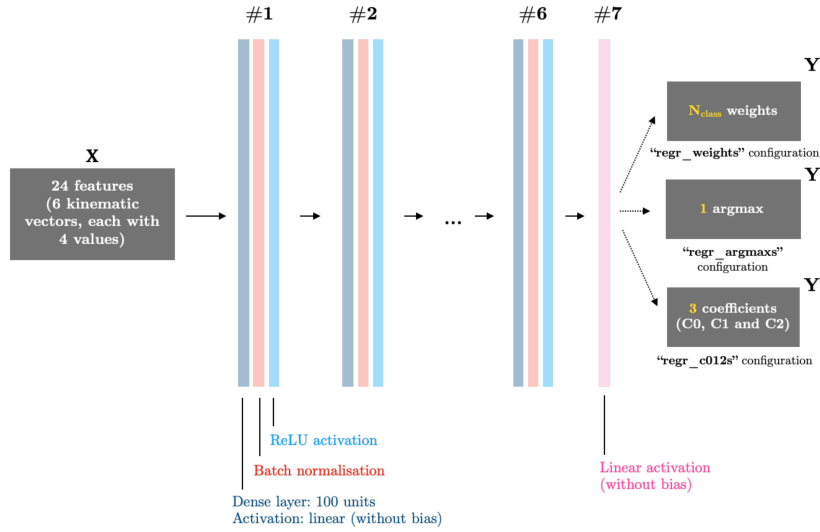


Figure 11: Architecture of regression models

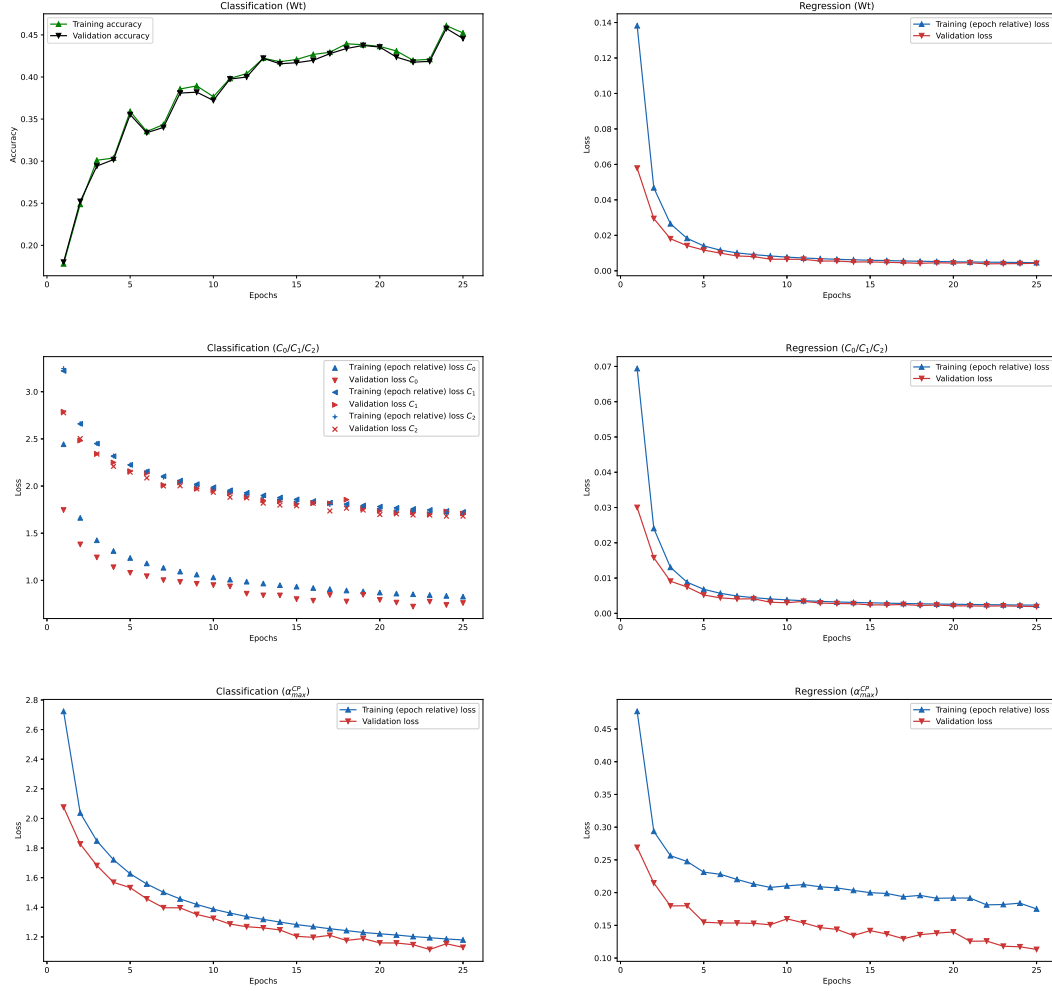


Figure 12: The DNN performance observed during the training process for *Variant-All*: accuracy for Classification:weights and loss for all the other models. For the classification, $N_{class} = 51$ classes were used.

A.2 Training

During the training process, we monitored accuracy, the difference between predicted and true values (mean, L_1 and L_2), and training epoch relative loss function value in the case of the multiclass classification model predicting the α_{max}^{CP} probability distribution. For other models, training and validation loss function values were recorded.

All DNN configurations (3 multiclass classification models and 3 regression models) have been trained for 25 epochs. Extending the training process to up to 120 epochs did not lead to significant changes in the performance of the models. During the training, model weights were saved for each epoch separately, and after the training, we used the "best" weights for evaluation. The "best" weights were those leading to the highest validation accuracy for the multiclass classification model predicting the α_{max}^{CP} probability distribution or the lowest loss function value for all the other DNN configurations.

Convergence can be observed for all the configurations trained. Figure 12 shows it for models trained on the *Variant-All* feature set.

A.3 Unweighted events

Event weights were stored as a two-dimensional matrix, in which rows represented particular events and columns represented α_{max}^{CP} hypotheses. We transformed the matrix into the one containing ones and zeroes by using a Monte Carlo approach: if an element was greater than or equal to a number generated using a uniform random generator, it was replaced by 1 or 0, otherwise.

Therefore, each column of the unweighted events matrix contained those events that statistically represented the corresponding hypothesis. The columns were then used as a mask for filtering all the events and getting only the ones belonging to a specified α_{max}^{CP} hypothesis class. The fact that the summed distribution of the filtered events depicted the chosen hypothesis can be observed in Figures 7 - 9.

A.4 Negative weights

DNN models made predictions on the unweighted events, but due to the lack of restrictions in some of the configurations regarding the sign of the obtained α_{max}^{CP} weights, some of the predictions (up to 10%) contained negative weights. Such predictions did not have any physical interpretation, as the models were supposed to provide probabilities. We rejected those events containing negative values, ensuring they were added to the summed distribution with zero weight. Vectors containing the summed distribution were then normalised to allow us to compare predictions with true values on the same diagram.

References

- [1] Dan Guest, Kyle Cranmer, and Daniel Whiteson. “Deep Learning and its Application to LHC Physics”. In: (2018). arXiv: 1806.11484 [hep-ex].
- [2] Giuseppe Carleo et al. “Machine learning and the physical sciences”. In: (2019). arXiv: 1903.10563 [physics.comp-ph].
- [3] Kim Albertsson et al. “Machine Learning in High Energy Physics Community White Paper”. In: (2018). arXiv: 1807.02876 [physics.comp-ph].
- [4] M. Kramer et al. “Prospects of measuring the parity of Higgs particles”. In: *Z. Phys. C* 64 (1994), pp. 21–30. DOI: 10.1007/BF01557231. arXiv: hep-ph/9404280 [hep-ph].
- [5] G. R. Bower et al. “Measuring the Higgs boson’s parity using tau $\rightarrow \ell \rho \nu$ ”. In: *Phys. Lett. B* 543 (2002), pp. 227–234. DOI: 10.1016/S0370-2693(02)02445-0. arXiv: hep-ph/0204292 [hep-ph].
- [6] Andre Rouge. “CP violation in a light Higgs boson decay from tau-spin correlations at a linear collider”. In: *Phys. Lett. B* 619 (2005), pp. 43–49. DOI: 10.1016/j.physletb.2005.05.076. arXiv: hep-ex/0505014 [hep-ex].
- [7] K. Desch, Z. Was, and M. Worek. “Measuring the Higgs boson parity at a linear collider using the tau impact parameter and tau $\rightarrow \ell \rho \nu$ decay”. In: *Eur. Phys. J. C* 29 (2003), pp. 491–496. DOI: 10.1140/epjc/s2003-01231-4. arXiv: hep-ph/0302046 [hep-ph].
- [8] Stefan Berge and Werner Bernreuther. “Determining the CP parity of Higgs bosons at the LHC in the tau to 1-prong decay channels”. In: *Phys. Lett. B* 671 (2009), pp. 470–476. DOI: 10.1016/j.physletb.2008.12.065. arXiv: 0812.1910 [hep-ph].
- [9] Stefan Berge, Werner Bernreuther, and Sebastian Kirchner. “Prospects of constraining the Higgs boson’s CP nature in the tau decay channel at the LHC”. In: *Phys. Rev. D* 92 (2015), p. 096012. DOI: 10.1103/PhysRevD.92.096012. arXiv: 1510.03850 [hep-ph].
- [10] Georges Aad et al. “Measurement of the CP properties of Higgs boson interactions with τ -leptons with the ATLAS detector”. In: *Eur. Phys. J. C* 83.7 (2023), p. 563. DOI: 10.1140/epjc/s10052-023-11583-y. arXiv: 2212.05833 [hep-ex].
- [11] Armen Tumasyan et al. “Analysis of the CP structure of the Yukawa coupling between the Higgs boson and τ leptons in proton-proton collisions at $\sqrt{s} = 13$ TeV”. In: *JHEP* 06 (2022), p. 012. DOI: 10.1007/JHEP06(2022)012. arXiv: 2110.04836 [hep-ex].
- [12] T. Przedzinski, E. Richter-Was, and Z. Was. “TauSpinner: a tool for simulating CP effects in $H \rightarrow \tau\tau$ decays at LHC”. In: *Eur. Phys. J. C* 74.11 (2014), p. 3177. DOI: 10.1140/epjc/s10052-014-3177-8. arXiv: 1406.1647 [hep-ph].
- [13] R. Józefowicz, E. Richter-Was, and Z. Was. “Potential for optimizing the Higgs boson CP measurement in $H \rightarrow \tau\tau$ decays at the LHC including machine learning techniques”. In: *Phys. Rev. D* 94 (9 Nov. 2016), p. 093001. DOI: 10.1103/PhysRevD.94.093001. URL: <https://link.aps.org/doi/10.1103/PhysRevD.94.093001>.
- [14] K. Lasocha et al. “Machine learning classification: Case of Higgs boson CP state in $H \rightarrow \tau\tau$ decay at the LHC”. In: *Phys. Rev. D* 100 (11 Dec. 2019), p. 113001. DOI: 10.1103/PhysRevD.100.113001. URL: <https://link.aps.org/doi/10.1103/PhysRevD.100.113001>.
- [15] K. Lasocha et al. “Deep neural network application: Higgs boson CP state mixing angle in $H \rightarrow \tau\tau$ decay and at the LHC”. In: *Phys. Rev. D* 103 (3 Feb. 2021), p. 036003. DOI: 10.1103/PhysRevD.103.036003. URL: <https://link.aps.org/doi/10.1103/PhysRevD.103.036003>.
- [16] I Goodfellow, Y. Bengio, and A Courville. *Deep learning*. MIT Press, Cambridge, MA, 2017.
- [17] Martín Abadi et al. *TensorFlow: Large-Scale Machine Learning on Heterogeneous Systems*. Software available from tensorflow.org. 2015. URL: <https://www.tensorflow.org/>.
- [18] K. Desch et al. “Probing the CP nature of the Higgs boson at linear colliders with tau spin correlations: The case of mixed scalar-pseudoscalar couplings”. In: *Phys. Lett. B* 579 (2004), pp. 157–164. DOI: 10.1016/j.physletb.2003.10.074. arXiv: hep-ph/0307331.

- [19] S. Jadach et al. “The tau decay library TAUOLA: Version 2.4”. In: *Comput. Phys. Commun.* 76 (1993), pp. 361–380. DOI: 10.1016/0010-4655(93)90061-G.
- [20] Torbjörn Sjöstrand et al. “An introduction to PYTHIA 8.2”. In: *Computer Physics Communications* 191 (2015), pp. 159–177. ISSN: 0010-4655. DOI: <https://doi.org/10.1016/j.cpc.2015.01.024>. URL: <https://www.sciencedirect.com/science/article/pii/S0010465515000442>.
- [21] N. Davidson et al. “Universal interface of TAUOLA: Technical and physics documentation”. In: *Computer Physics Communications* 183.3 (2012), pp. 821–843. ISSN: 0010-4655. DOI: <https://doi.org/10.1016/j.cpc.2011.12.009>. URL: <https://www.sciencedirect.com/science/article/pii/S0010465511003973>.
- [22] Z. Czyżula, T. Przedzinski, and Z. Was. “TauSpinner Program for Studies on Spin Effect in tau Production at the LHC”. In: *Eur.Phys.J. C* 72 (2012), p. 1988. DOI: 10.1140/epjc/s10052-012-1988-z. arXiv: 1201.0117 [hep-ph].
- [23] T. Przedzinski, E. Richter-Was, and Z. Was. “Documentation of *TauSpinner* algorithms: program for simulating spin effects in τ -lepton production at LHC”. In: *Eur. Phys. J. C* 79.2 (2019), p. 91. DOI: 10.1140/epjc/s10052-018-6527-0. arXiv: 1802.05459 [hep-ph].
- [24] V. Cherepanov, E. Richter-Was, and Z. Was. “Monte Carlo, fitting and Machine Learning for Tau leptons”. In: *SciPost Phys. Proc.* 1 (2019), p. 018. DOI: 10.21468/SciPostPhysProc.1.018. arXiv: 1811.03969 [hep-ph].
- [25] François Chollet et al. *Keras*. <https://keras.io>. 2015.
- [26] Pauli Virtanen et al. “SciPy 1.0: Fundamental Algorithms for Scientific Computing in Python”. In: *Nature Methods* 17 (2020), pp. 261–272. DOI: 10.1038/s41592-019-0686-2.
- [27] Sergey Ioffe and Christian Szegedy. *Batch Normalization: Accelerating Deep Network Training by Reducing Internal Covariate Shift*. 2015. eprint: arXiv:1502.03167.
- [28] Diederik P. Kingma and Jimmy Ba. *Adam: A Method for Stochastic Optimization*. 2014. eprint: arXiv:1412.6980.